Egyptian Journal of Chemistry

http://ejchem.journals.ekb.eg/

The Catalytic Role of L-cysteine During Electrolytic Zinc Deposition

Ahmed diaa .A .Abdelsalam[1] , Hamdy.H. Hassan[1] , Badr.A. Elsayed[2] , Magdy.A.M. Ibrahim[1]*
[1] Department of Chemistry, Faculty of Science, Ain Shams University, Abbassia, Cairo 11566, Egypt
[2]Department of Chemistry, Faculty of Science, Al-Azhar University, Cairo11651, Egypt.

Abstract

In this study, utilizing L-Cys as a complexing agent in an acid-sulphate zinc bath led to significant improvements. Using cathodic current efficacy, polarization curves, in situ anodic linear stripping voltammetry, i-t transient, and macrothrowing power, it has been determined how Cys affects zinc electrodeposition from a sulphate solution. Due to L-Cys' catalytic impact on the reduction of Zn^{+2} ions, the i-E curve and potential of zinc deposition significantly move in the direction of more positive values when L-Cys is present. The kinetic data show that in the existence of Cys, both the Tafel slope (β_C) and the exchange current (i_o) are higher (496.1– 616.3 mV decade^{-1}), (0.0034 Acm^{-2}) than without Cys (429.2 mV decade^{-1}), (0.0017 Acm^{-2}) respectively. As the concentration of L-Cys rises, the exchange current density significantly increases. Moreover, the limiting current was greatly increased by the existence of L-Cys. The consistent values of the transfer coefficient αc, however, suggest that the presence of Cys has no effect on the Zn electrodeposition process. Both the Wagner number and the macrothrowing power are reduced with the inclusion of Cys. The surface appearance and composition of zinc deposits have been examined using SEM and EDX in the present and absent Cys.

Keywords: Zinc electrodeposition; polarization curves; L-cysteine; chronoamperometry; anodic stripping.

1. Introduction

Recently, electrodeposition has been considered among the most widely utilized applied processes for the fabrication of zinc coatings with the appropriate look and characteristics. Electrodeposition of the objects was carried out to achieve a hard shape with an appealing surface that resists corrosion. It is also used in the purification of metals, such as in copper electrorefining [1], the separation of the metals, or, as in electrotyping, to replicate the ions on the surface from a bulk. Nickel, zinc, chromium, copper, cadmium, tin, gold, and silver are the metals most often used in plating on surfaces. In many respects, electrodeposited zinc will be utilized to protect steel against erosion and corrosion [2-5]. Energy storage systems rely heavily on zinc and its alloys because of their practical relevance. Generally, there are two electrolytic solutions for zinc electrodeposition, an acid bath [6-10], and an alkaline cyanide bath [11]. Because of their low throwing power (TP), acid plating baths are not frequently utilized and do not create a brilliant coating [12]. Baths of cyanide plating are often used for corrosion resistance and ornamental plating because of their excellent TP but they are not eco-friendly [13]. Recently, research has been oriented toward electrodeposition with non-toxic electrolytes [14]. To boost the attitude of deposits and optimize the surface topography and effectiveness of electrodeposited zinc, numerous chemical substances have been proposed as additives [15-22]. One of the easiest and most popular ways to raise the electrolytic baths' throwing power and deposit quality is to add organic compounds to the electrolytic bath. The polarizable or charged groups found in organic additives are typically based on N- or S-containing groups, such as amines, proteins, alkaloids, mercaptans, sulfonates, and sulfides, Cysteine was previously used as an additive during Ni deposition [23-25]. Zinc was electrodeposited from an acid sulphate bath in the current investigation using Cys as a complexing agent. Therefore, the present study aimed to characterize the acid solution based on Cys electrolytes as well as focus on understanding the mechanism of zinc deposition.

2. Experimental

Both steel and platinum sheets were applied for electrolytic deposition as a cathode and anode, respectively, with a size of 2.3 x 3 cm. 3.0 cm separated the cathode from the anode. The electrolytic bath contains: 0.15M $ZnSO_4.7H_2O$, 0.2M Na_2SO_4, and Cys ($HO_2CCH(NH_2)CH_2SH$) (0.05-0.2 M).
By adding 1:1 H_2O/H_2SO_4, the electrolyte pH has been adjusted. Most of the tests were conducted at pH 2.0- 4.0. The efficacy of the cathodic current, CCE%, and cell utilized had been outlined before [3]. All studies were performed using an unstirred solution, and the bath temperature was 25 ± 2°C. For potentiodynamic measurements, a Potentioscan Wenking POS73 was utilized, operated by a personal computer. The software packages supplied by POS73 were used for measuring and analyzing the data. Every potential was measured using a silver/silver chloride reference electrode. At a scan rate of 5 mVs^{-1}, the potential was swept from -0.5 V to -1.5 V to detect the potentiodynamic polarization. A cell containing three electrodes was used for electrochemical measurements. A glassy carbon (GC, 0.125

cm^2) implanted in a polypropylene tube served as the working electrode. The GCE was cleaned with 0.25 mm diamond paste before each run and then rinsed with distilled water multiple times. The counter-electrode was a Pt wire. The anodic stripping voltammetry setup (ALSV) had been mentioned before [19, 24]. The current–time transients were performed with various step potentials and with various concentrations of Cys. The solution macrothrowing power (TP) has been measured using the rectangular Haring–Blum perspex cell as described elsewhere. An AMETEK Advance microanalysis SEM and EDX were utilized to characterize the surface topography and the composition of the zinc deposits.

3. Results and discussion
3.1 Efficacy of the cathodic current
The efficacy of the cathodic current (CCE%) was stimulated by simply obeying Faraday's laws (1),

$$CCE\% = W/W_t \times 100 \quad (1)$$

where W and W_t are the practical and theoretical weights of zinc deposits, respectively. Throughout the Zn^{2+} ion deposition, simultaneous releases of hydrogen ions have been observed. Table 1 displays how changing the Cys concentration in the electrolytic zinc solution affects the CCE%. The findings demonstrated a clear drop in CCE% with rising Cys concentrations (from 98.6 % to 80.9%). This is due to Zn^{2+} ions forming a soluble complex with Cys according to the following equilibrium [26],

$$Zn^{+2} + L^- \longrightarrow Zn(L)^+ \quad (2)$$
$$K = [Zn(L)^+]/ [Zn^{+2}] [(L)^-] \quad (3)$$

where K is the equilibrium constant. Due to the complexation of Zn^{+2} with Cys molecules, increasing the concentration of Cys in the bath lowers the concentration of free Zn^{2+} ions, so both the CCE% and the concurrent hydrogen reaction drop. The following reaction may usually explain the zinc deposition from simple zinc ions:

$$Zn^{+2} + 2e^- \longrightarrow Zn \quad (4)$$

From independent side reactions:

$$Zn(L)^+ + 2e^- \longrightarrow Zn^0 + L^- \quad (5)$$

Throughout the Zn^{2+} ions deposition in the existence of 0.1 M Cys, the impact of applied current (0.025 to 0.2 mA cm^{-2}) on the CCE% was investigated. The CCE% has values ranging from 80.1-83.2% as shown in Table 1. However, at current densities above 0.1 mA cm^{-2}, the deposit burned. Therefore, 0.055 mA cm^{-2} was taken as the optimum current density since it gives a satisfactory deposit with a good CCE%. Moreover, Table 1 clarifies that as the pH is changed from pH 2.0 to pH 4.0, the CCE% increases from 81.7 to 85.1. At pH ≥ 5.0, the solution becomes turbid because zinc hydroxide forms at this pH. The influence of bath temperatures (25 – 55°C) on the CCE% is given in Table 1. The findings show that raising the temperature slightly reduced the CCE% because of the increased simultaneous H$_2$ evolution at high temperatures.

3.2 The i/E curves
The i/E polarization diagrams were measured in the absence and existence of Cys (0.05 - 0.20 M) during the electrodeposition of zinc on steel substrates, and the data is shown in Fig. 1. The polarization curves significantly shift toward lower negative potential values when Cys is present. The presence of a variety of limiting currents (i$_{lim}$) is another feature of polarization curves. According to Fig. 1 inset, this limiting current density increases noticeably as Cys concentrations rise. It appears that the complex generated with the reduction of Zn^{+2} ions is the one that caused the effect of Cys to be tied to Zn^{+2} ions. This shows that Cys won't impede the active sites of zinc deposition on the electrode surface but rather will speed up zinc deposition on the cathode surface. Fig. 2 illustrates the impact of pH (2.0 – 4.5) on the i/E polarization curves. The i/E curves have changed adversely with increasing pH. Increasing the pH increases the limiting current (Fig. 2 inset). Fig. 3 explores the impact of temperature on the i/E curves. A rise in bath temperature leads to a depolarizing effect due to its impact on the reducible ions' activation overpotential. The relative quantity of both complex and uncomplexed Zn^{+2} ions in the solution may also alter as the temperature rises. Uncomplexed Zn^{+2} ion concentrations rise as the temperature rises. Tafel constants were obtained from the relevant log i-E curves to get quantitative data about the kinetics of zinc deposition in the presence of Cys. Additionally, to the electrokinetic parameter values, i$_o$ (exchange current densities), and α$_c$ (the transfer coefficient) shown in Table 2, the Tafel slopes (β$_C$) were determined from the straight lines in the absence and presence of Cys. The Tafel lines were extrapolated to zero overpotential to produce the i$_o$ for zinc deposition. The results show that the β$_C$ increases with increasing Cys concentrations, but the α$_c$ remains somewhat constant. In addition, with increased Cys concentration, the i$_o$ is significantly increased. The i$_o$ is often enhanced by an accelerated electrochemical reaction [27]. The analysis of the i/E profiles (Fig. 1), indicates that Cys improves the rate of Zn^{+2} electron transport through the EDL. On the other hand, increasing the pH values increases the β$_C$ and the i$_o$ (Table 2). Increasing temperature raises the β$_C$ and the i$_o$. Here, it should be noted that any aspect that reduces cathodic polarization (e.g., Cys concentrations, pH, or temperature) increases the β$_C$ and vice versa. The values of α$_c$ are mostly invariant and nearly constant in all the examples examined. This shows that the prior variable has no impact on the electrodeposition of Zn^{2+} ions under these circumstances, In this study, it is presumed that Zn^{2+} ions prefer an octahedral geometry in water [$Zn(H_2O)_6$]$^{2+}$, and L-Cys exists predominantly as a zwitterion essentially at pH 2.05 to 8.0 [28]. The molecule's carboxyl group gives L-Cys its ability to form complexes. In the coordination sphere of the zinc ions, L-Cys replaces water molecules when L-Cys is introduced to water:

$$[Zn(H_2O)_6]^{2+} + L\text{-}Cys = [Zn(H_2O)_5Cys]^{2+} + H_2O \quad (6)$$
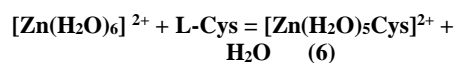
The pH of the solution affects L-Cys' coordination mode with the metal core. Since there will be a significant quantity of free Zn^{2+} ions and a limited amount of coordination spheres with L-Cys in the solution based on our experimental concentrations, the polarization curves will move towards more noble potentials, i.e., L-Cys stimulates Zn^{2+} ion electro-reduction. Additionally, L-Cys in its zwitterion state may be thought of as an active species among the hydrated Zn^{2+} ions that can move across the Zn-hydrated complex and facilitate Zn^{2+} ion reduction.
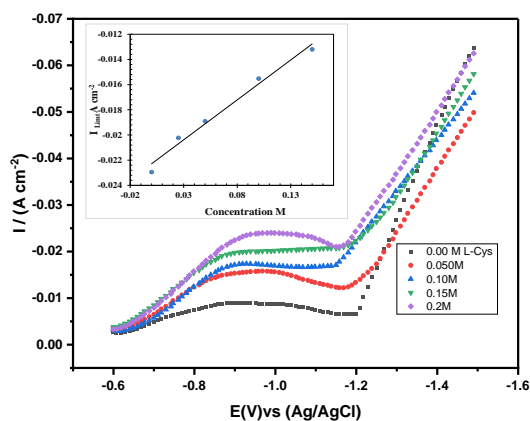
Fig 1 Potentiodynamic polarization curves during zinc deposition on steel substrate from the acid bath in the absence and presence of Cys, inset is the relationship between i_{lim} and concentration of Cys.
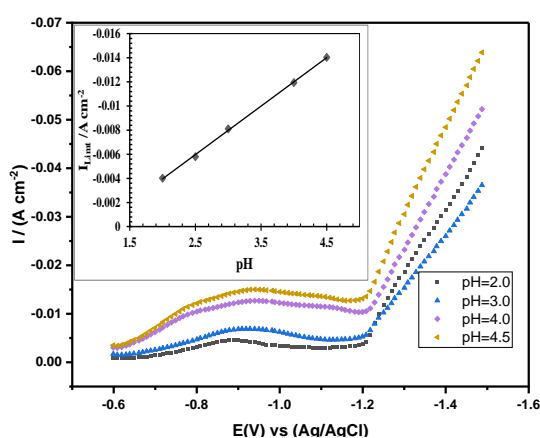

Fig 2 Potentiodynamic polarization curves during zinc deposition from the acid bath in the presence of Cys (0.1 M) at different pH, inset is the relationship between i_{lim} and pH.
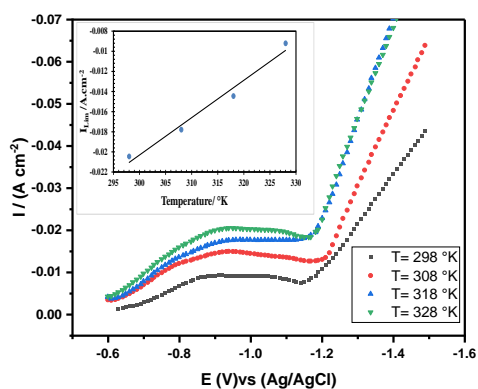

Fig 3 Potentiodynamic polarization curves during zinc deposition from the acid bath in the presence of Cys (0.1 M) at different temperatures, inset is the relationship between i_{lim} and temperature.

3.3 Anodic linear stripping voltammetry (ALSV)

ALSV was accomplished as follows: the first step is depositing zinc on a GCE at -1.3 $V_{Ag/AgCl}$ for 100 s. The second step is that the potential was linearly scanned in the direction of the lesser potential without removing the

electrode from the solution (i.e., in situ) or altering the existing circumstances, an anodic stripping voltammogram was captured (Figs. 4 a, b, and c). As shown in Fig. 4a, a series of voltammetric studies were performed by depositing zinc on GCE at a predefined constant deposition potential, both with and without Cys. The peaks appear in such a diagram, corresponding to what has been deposited from zinc potentiostatically on the GCE. There was no sign of any lingering zinc or zinc oxide. As a result of the consumed zinc ion during anodic stripping, which could be used to determine the current efficacy of zinc deposition, i.e., the amount of zinc deposited is equal to the area under the peak. By adding Cys to the bath (0.05 to 0.2M), the height and the anodic peak area were decreased significantly. This means that zinc deposition on GC is inhibited in the presence of Cys. In reverse to what happened on the steel surface, a catalytic effect was observed during zinc plating on the steel surface. The substrate surface thus plays a significant role in the electrodeposition process. Another series of ALSV was carried out, but with different values of deposition potentials, as shown in Fig. 4b. As the potential of zinc deposition was made less noble, the peak and the area under the stripping peaks increased, which means a high amount of zinc was deposited at high negative potentials. On the other hand, increasing the time of deposition at a constant deposition potential (-1.3 V) sharply enhances the peak and the area under the peak (Fig. 4c) referring to a large amount of zinc formed as the deposition time increases.
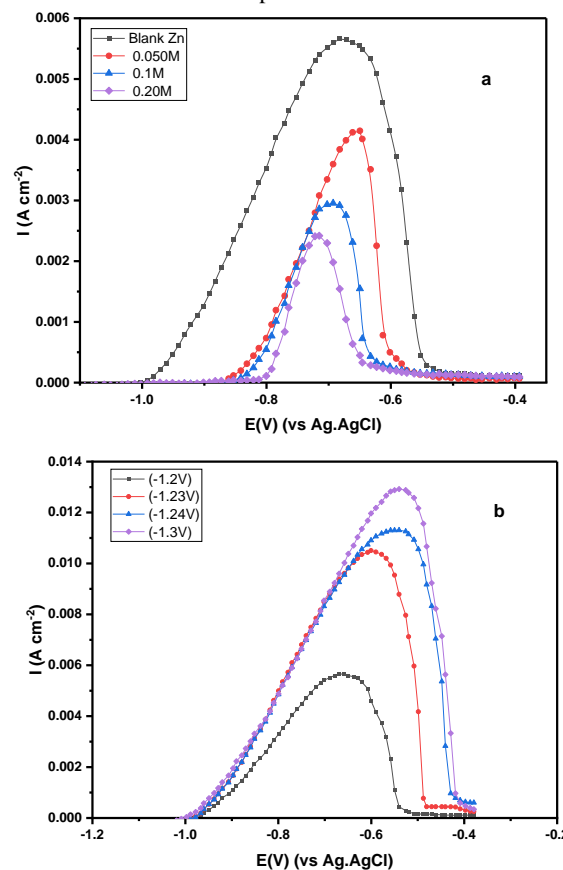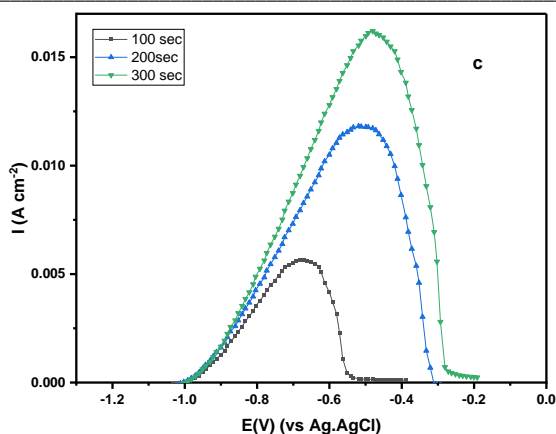
Fig. 4 ALSV recorded at GCE, scan rate 5 mVs⁻¹.

3.4 Chronoamperometric analysis

Chronoamperometric analysis (current-time transients) was taken to comprehend the early zinc deposition's nucleation and growth processes. The results are displayed in Figs. 5a, b, and c. Maximum currents are present in the i-t transients observed throughout the reduction of Zn^{+2} ions in both the absence and existence of Cys at a deposition potential of -1.3 $V_{Ag/AgCl}$. The current enhances sharply, achieving a maximum value, then decreases monotonically and finally, reaches a steady state value (Fig. 5a). The current transients level off when the exposed surface reaches saturation. The maximum current decreases significantly with increasing Cys concentrations. When the electroactive region grows due to either immediate expansion (each independent nucleus grows) or progressive growth (an increase in the total number of nuclei), the ascending portion of the curve takes this increase in current into account. However, the decline in the current followed the first region, which is short and connected to the electrical double-layer charge. On the other hand, Fig. 5b shows the i–t relation at different cathodic step potentials. When the cathodic potential is lowered, the values of the observed instantaneous current increase. Another series of current-time transients were reported at various pH values. The maximum current increases as the pH value rises (Fig. 5c). The zinc deposit develops under experimental conditions by a mechanism where instantaneous nucleation is followed by three-dimensional growth under charge transfer control [11], as shown by the extremely strong linearity of the $i^{1/2}$ graphs against time t in the inset of Fig. 5. These lines' slopes are directly related to the charge transfer rate constant.

The concept that the development of zinc metal under these conditions is a diffusion-controlled process that complies with equation (7) (Cottrell equation) is supported by graphing the current density i vs. $t^{-1/2}$ during the decreasing portions of the current transients

$$I = P/t^{1/2} \quad (7)$$

where,

$$P = nFcD^{1/2} / II^{1/2} \quad (8)$$

where c is the concentration, D is the diffusion coefficient of the disseminated species, and n is the number of electrons that were exchanged. Thus, it is possible to hypothesize that zinc deposits form through a nucleation and growth mechanism that is diffusion-controlled.
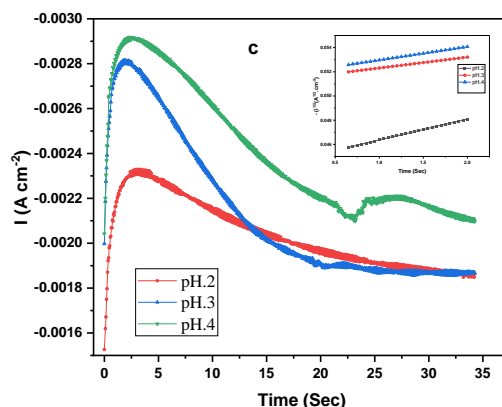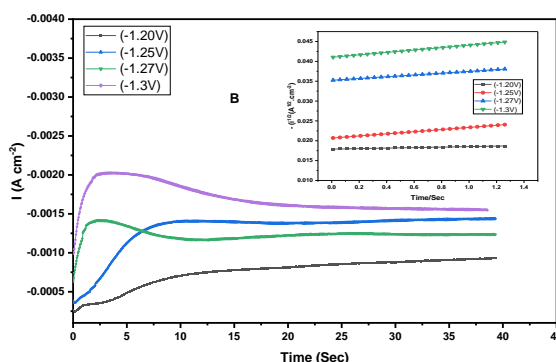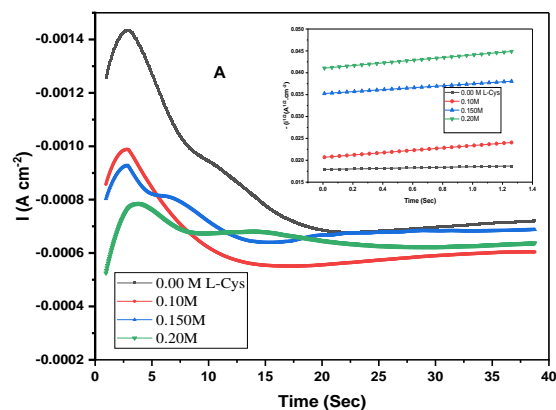

Fig 5 Current–time transients curves recorded at GCE in the absence and presence of Cys at -1.3 V (a), at 0.1 M Cys and different applied potentials (b), at 0.1 M Cys and different pH (c).

3.5 Macrothrowing power and throwing index

Throwing power is the capacity of the electrolytic solution to provide a uniform deposit on an object of irregular shape. The Haring-Blum cell was used to calculate the macrothrowing power (TP) of the zinc plating bath both with and without Cys. The TP values determined using Field's empirical method at a 1:3 distance ratio are displayed in Table 3 [27]. Analyzing the data indicates that the bath's TP% is 28.24%. The TP is significantly reduced by Cys addition, dropping to 12.28% at 0.15M Cys. The TI is a different way to express the plating bath's TP. The metal dissemination ratio M and the linear ratio L (1:1 to 1:5) were

plotted to calculate the TI, as shown in Table 3. The TP of the bath is measured by the TI, which is the reciprocal of the slopes of these lines. In this diagram, a bath with a low TP would result in a very steep line, whereas an ideal solution would result in a horizontal line at L = 3.0. There are several benefits to the manifestation of TP as TI. One number, for instance, that is characteristic of several different linear ratios is discovered. Additionally, TI is calculated from several experimental spots, which reduces measurement errors overall. The effects of the following variables (concentration, pH, and temperature) on the bath are depicted in Fig. 6 (a, b, and c). In the absence of Cys, the impact of concentration has a TI value of 3.83. The bath's TI drops to 2.70 when Cys is added. As shown in Fig. 1, a drop in the polarization curve may be the cause of the decline in TI. The TP and TI of the sulphate bath were usually negatively impacted by all factors that decreased polarization. Table 3 shows that the addition of Cys has no appreciable impact on electrolyte conductivity. Based on the most recent findings, which demonstrate a decline in TP in the presence of Cys, temperature exhibits the same pattern as a concentration influence on pH in the opposite direction [27].

3.6 Wagner's number

The Wagner number (Wa) [29, 30], which compares polarization resistance to solution resistance, serves as a measure of electrodeposition homogeneity. Despite non-uniform geometry, the current distribution, as it stands now, becomes more uniform the larger it is. The equation that defines the Wagner number (9)

$$a = \frac{K}{L} \left(\frac{d\eta}{di}\right) \qquad (9)$$

where $(d\eta/di)$ is the slope of the potential-current density curve, L is the electrode's width (3.0 cm), and k is the electrical conductivity of the solution. Table 3 contains the Wagner numbers for various curves. The findings demonstrate that, despite strong agreement between the TP, TI, and Wagner statistics, the distribution of current density gets smaller when the Wagner number drops. The current distribution, along with the TP and TI, becomes less uniform the lower the Wagner number.
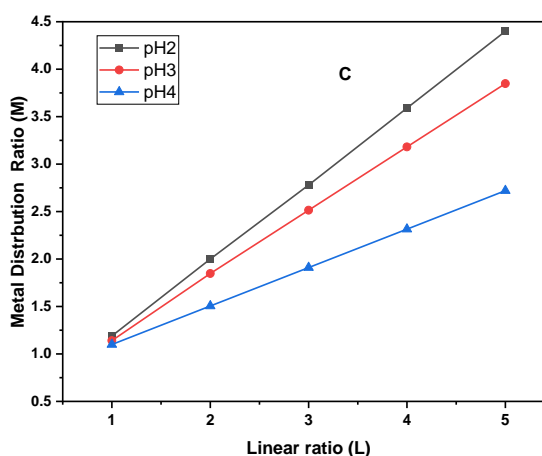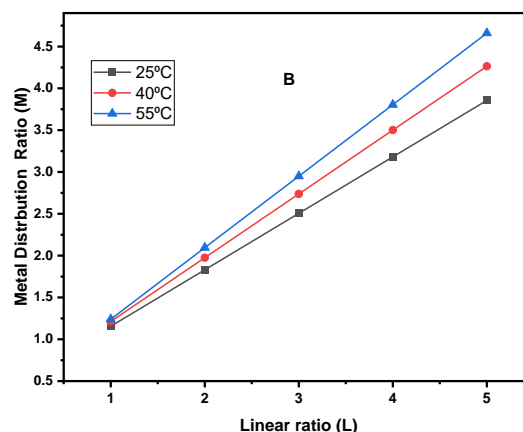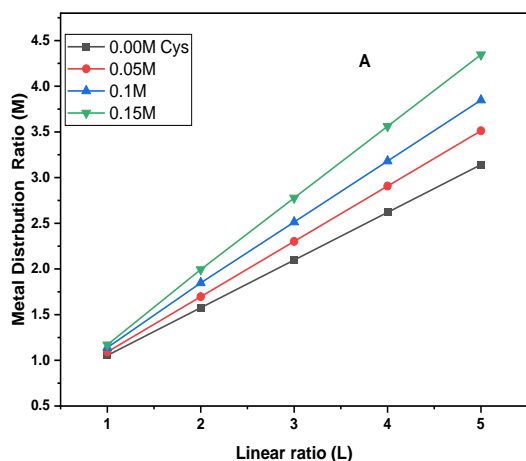
Fig 6 Throwing index of Zn bath (A: effect of concentrations L-Cysteine, B: effect of Temperature at 0.1 M Cys, and C: effect of different pH).

3.7 Surface morphology

SEM was used to study the surface morphology of the zinc deposit on the steel plate. According to the SEM data, the zinc formed big grains when it was deposited at 0.055 mA cm^2, pH 2.0, for 10 min., typically the usual zinc crystals [3, 19, 27], as shown in Fig. 7a. But when Cys was added, the morphology underwent a significant alteration. Cys (0.1M) creates a surface with uniform fine particles. elongated, shaped grains of similar size, as shown in Fig. 7b, covering the entire cathode surface, were observed. It appears that when Cys is present, the nucleation rate outpaces the growth rate, resulting in deposits that are more densely packed and have smaller grains, but when Cys is absent, the growth rate outpaces nucleation, leading to large grain deposits. But when the Cys concentration is raised to 0.2 M, an uneven grain aggregation surface morphology results (Fig. 7c). The microstructure of the deposited zinc that was obtained from the sulphate bath in both the presence and absence of Cys was examined using Energy Dispersive X-ray Analysis (EDX), as shown in Figs. 8a and b. The appearance of extra peaks in the presence of Cys at 5.5 kev indicates an extra amount of Zn deposits because of the catalytic effect of Cys during the Zn deposition.

_____

Table 1 The effect of L-Cys concentrations, pH, temperatures, and current densities on the CCE%

L-Cys(M)	CCE%	pH	CCE%	T/ºC	CCE%	i(mA/cm²)	CCE%
0.00	98.6	2.0	81.7	25.0	85.2	0.025	82.1
0.05	87.1	3.0	83.2	35.0	83.1	0.055	83.2
0.10	85.2	4.0	85.1	45.0	82.0	0.100	81.1
0.15	82.6	-	-	55.0	80.0	0.150	80.1
0.20	80.9	-	-	-	-	0.200	80.2

Table 2 Tafel kinetic parameters for zinc deposition

Variable	β_C (mV decade^{-1})	i_o A cm^{-2}	α_c
L-Cys/M			
0.00	429.2	0.0017	0.07
0.05	496.1	0.0022	0.07
0.10	533.9	0.0031	0.06
0.15	590.7	0.0033	0.06
0.20	616.3	0.0036	0.06
pH			
2.0	533.9	0.0005	0.06
2.5	543.0	0.0009	0.06
3.0	560.0	0.0010	0.06
3.5	571.2	0.0023	0.06
4.0	585.8	0.0039	0.06
Temp. °C			
25	532.1	0.0009	0.06
35	549.5	0.0017	0.06
45	582.1	0.0019	0.06
55	595.3	0.0103	0.06

Table 3 The effect of Cys concentration, pH, and temperature on TP%, TI, and W_a

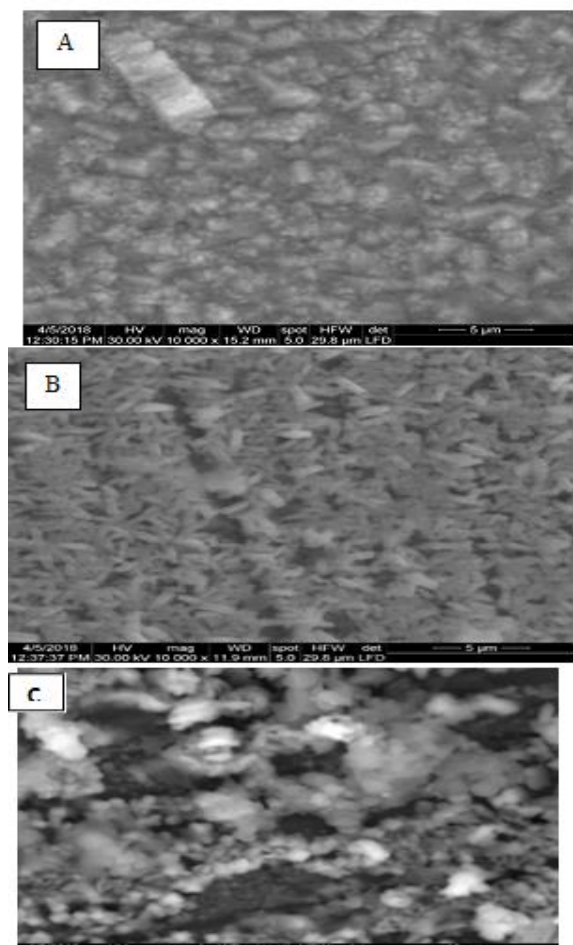| Variable	TP%	TI	W_a	Conductivity
	%			mS.cm^{-1}
L-Cys/M				
0	28.2	1.9	12.3	19.25
0.05	19.4	1.7	10.6	19.28
0.1	14.0	1.5	9.5	19.31
0.15	3.4	1.3	8.1	19.34
pH				
2	5.8	1.2	8.0	19.20
3	14.0	1.5	9.5	19.25
4	37.9	2.5	15.9	19.29
Temperature/°C				
25	13.1	1.5	9.5	19.20
45	7.2	1.3	8.4	19.23
55	1.3	1.2	7.5	19.26

_____

Fig. 7 SEM for zinc deposited from; A: blank, B: 0.1M Cys, C: 0.15 M Cys.
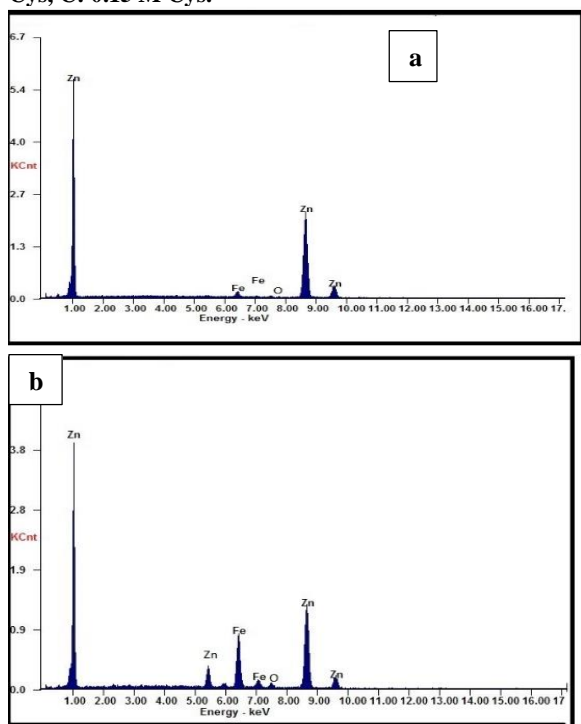

Fig.8 EDX analysis of Zn deposits in the absence (a) and presence of 0.1 M Cys(b).

4. Conclusion

Zinc depositions were effectively produced from an aqueous complex Cys sulphate bath on a steel substrate. Due to L-Cys' catalytic impact on the reduction of Zn2+ ions, the i-E curve and potential of zinc deposition significantly change in the direction of more positive values when L-Cys is present. The kinetic data show that in the presence of Cys, both the Tafel slopes (βC) and the exchange current density (io) are higher (496.1– 616.3 mV decade^{-1}), (0.0034 Acm^{-2}) than without Cys (429.2 mV decade^{-1}), (0.0017 Acm^{-2}) respectively. As the concentration of L-Cys rises, the exchange current density significantly increases. Moreover, the limiting current was greatly increased in the presence of L-Cys. The consistent values of the transfer coefficient αc, however, suggest that the presence of Cys does not affect the Zn electrodeposition process. Both the Wagner number and the macrothrowing power are reduced with the inclusion of Cys. The measurement of chronoamperometry showed that Zn growth is a diffusion-controlled process. The findings of the EDX Energy Dispersive X-ray analysis and the SEM indicated that the Cys modified the crystal structure of electrodeposited zinc.

5. Conflicts of interest
"There are no conflicts to declare".

6. Formatting of funding
Sources Self

8. References
1. Hoppstock K, et al (1994) Purification of analytical reagents by constant-current electrodeposition of heavy metals at ultra-trace levels from highly concentrated salt solutions. Analytica Chimica Acta 294:57-68.
2. Kordesh K and Weissenbacher M (1994) Rechargeable alkaline manganese dioxide/zinc batteries. Journal of Power Sources 51:61-78.
3. Ibrahim MAM and Bakdash R (2014) Zinc coatings of high hardness on steel by electrodeposition from glutamate complex baths. Transactions of the IMF 92:218-226.
4. Liu H., et al (2009) Preparation of superhydrophobic coatings on zinc as effective corrosion barriers. ACS Applied Materials & Interfaces 1(6):1150-1153.
5. Müller S, Holzer F and Haas O (1998) Optimized zinc electrode for the rechargeable zinc–air battery. Journal of Applied Electrochemistry. 28(9):895-898.
6. Trejo G et al (2001) Influence of polyethoxylated additives on zinc electrodeposition from acidic solutions. Journal of Applied Electrochemistry. 31(60):685-692.
7. Mouanga M, et al (2006) Influence of coumarin on zinc electrodeposition. Surface and Coatings Technology. 201(3-4):762-767.
8. Shivakumara S, et al (2007) Effect of condensation product on electrodeposition of zinc on mild steel. Bulletin of Materials Science. 30(5):463-468.
9. Naik, YA, Venkatesh TV and Nayak PV (2002), Electrodeposition of zinc from chloride solution. Turkish Journal of Chemistry, 26(5):725-734.
10. Fayard L., Bizouard V, Feynerola V, Schneider H, Turpin C (2923), Equivalent electrical model for high current density zinc electrodeposition:Investigation

through polarization curves and electrochemical impedance spectroscopy, International Journal of Electrochemical Science. 18:100185.

11. Bari D, GA, Schlesinger M, and Paunovic M (2000) Modern electroplating. New York, M. Schlesinger and M. Paunovic, Eds., John Wiley & Sons, Inc.

12. Ibrahim, MAM (2008), Zinc Coatings on Steel by Electrodeposition from Complexing Alkaline Ammoniacal Baths. J. Appl. Surf. Finish. 3:89-98.

13. Lowenheim FA and Senderoff S (1964) Modern electroplating. Journal of the Electrochemical Society. 111(11):262C.

14. Xia X, Zhitomirsky I, and McDermid JR (2009), Electrodeposition of zinc and composite zinc–yttria-stabilized zirconia coatings. Journal of Materials Processing Technology. 209(5):2632-2640.

15. Liu Z, El Abedin SZ, and Endres F (2015), Electrochemical and spectroscopic study of Zn (II) coordination and Zn electrodeposition in three ionic liquids with the trifluoromethylsulfonate anion, different imidazolium ions and their mixtures with water. Physical Chemistry Chemical Physics. 17(24):15945-15952.

16. Torrent-Burgués J and Guaus E (2007) Effect of tartaric acid in the electrodeposition of zinc. Journal of applied electrochemistry. 37:643-651.

17. Zhang D, et al (2020) Electrodeposition of zinc in aqueous electrolytes containing high molecular weight polymers. Macromolecules. 53(7):2694-2701.

18. Sajadi S (2010) Metal ion-binding properties of L-glutamic acid and L-aspartic acid, a comparative investigation. Natural Science. 2(02):85.

19. Ibrahim M.A.M. and EM Omar (2013) Synergistic effect of ninhydrin and iodide ions during electrodeposition of zinc at steel electrodes. Surface and Coatings Technology. 226:7-16.

20. Onkarappa NK et al (2020), Influence of additives on morphology, orientation and anti-corrosion property of bright zinc electrodeposit. Surface and Coatings Technology. 397:126062.

21. Elsayed EM and Shenouda AY (2022) Studies on Electrodeposition of Zinc Selenide and Zinc Telluride and Their Photoelectrochemical Cell Behavior. Egypt. J. Chem. 65(5) 623-633.

22. H. H. Shaarawy, H.S. Hussein, Mona A. Abdel-Fatah, Nabila H. Hussien, and S.I.Hawash (2021). Electrolytic Generation of Nickel Hydroxide and Nickel Oxide Nanoparticles for Advanced Applications. Egypt. J. Chem. 64(10) 5903 – 5913.

23. Kolonits T, et al (2020) Improved hardness and thermal stability of nanocrystalline nickel electrodeposited with the addition of cysteine. Nanomaterials. 10(11):2254.

24. El Boraei, NF (2022), Synergistic effect of L-cysteine and iodide ions during electrodeposition of nanocrystalline nickel from a Watts bath. Transactions of the IMF. 100(2):72-84.

25. Han K, and Fang F (1996) Effect of cysteine on the kinetics of electroless nickel deposition. Journal of Applied Electrochemistry. 26:1273-1277.

26. Cherifi K, et al (1990) Transition metal complexes of L-Cysteine containing Di-and Tripeptides. Journal of Inorganic Biochemistry. 38(1):69-80.

27. Ibrahim MAM, Improving the throwing power of acidic zinc sulfate electroplating baths. Journal of Chemical Technology & Biotechnology. 75(8):745-755.

28. Pace N J and Weerapana E (2014), Zinc-binding cysteines: diverse functions and structural motifs. Biomolecules. 4(2): p. 419-434.

29. Wagner C (1951) Theoretical analysis of the current density distribution in electrolytic cells. J Electrchem Soc. 98:116-128.

30. Marshall SL and Wolf SK (1998) Analysis of terminal effects in rectangular electrochemical cells. Electrochim Acta. 43:405-415.

31. Gomes A and Silva PMda (2006) Pulsed electrodeposition of Zn in the presence of surfactants. Electrochimica Acta. 51(7): 1342-1350.